

# A deformation gradient decomposition method for the analysis of the mechanics of morphogenesis

José J Muñoz<sup>a,b</sup>, Kathy Barrett<sup>c,d</sup>, Mark Miodownik<sup>a,\*</sup>

<sup>a</sup>*Materials Group, Div. Engineering, King's College London, UK*

<sup>b</sup>*Current address: Dep. of Appl. Mathematics III. Univ. Polit. Catalonia,  
Barcelona, Spain*

<sup>c</sup>*Dep. of Anatomy and Developmental Biology, Univ. College London, UK*

<sup>d</sup>*Dep. of Biochemistry and Molecular Biology. Univesity College London, UK*

---

## Abstract

A new finite element model is proposed for the analysis of the mechanical aspects of morphogenesis and tested on the biologically well studied gastrulation phenomenon, in particular ventral furrow invagination of the *Drosophila melanogaster* embryo. A set of mechanisms are introduced in the numerical model, which lead to the observed deformed shapes. We split the total deformation into two parts: an imposed active deformation, and an elastic deformation superimposed onto the latter. The active deformation simulates the effects of apical constriction and apico-basal elongation. These mechanisms are associated with known gene expressions and so in this way we attempt to bridge the well explored signalling pathways, and their associated phenotypes in a mechanical model. While the former have been studied in depth, much less can be said about the forces they produce and the mechanisms involved. From the numerical results, we are able to test different plausible

mechanical hypotheses that generate the necessary folding observed in the invagination process. In particular, we conclude that only certain ratios between both modes (apical constriction and apico-basal elongation) can successfully reproduce the invagination process. The model also supports the idea that this invagination requires the contribution of several mechanisms, and that their redundancy provides the necessary robustness.

*Key words:* invagination, *Drosophila*, finite elasticity, finite elements.

---

## 1 Introduction

The first stages of embryonic development of *Drosophila* involve the formation of the epithelium, (external layer of cells in the blastoderm that surround the yolk). Subsequently, these cells undergo a set of major changes in shape and topology, namely invagination on the ventral side and at the posterior end, which gives rise to the mesoderm and midgut (Parks and Wieschaus, 1991; Costa et al., 1994; Leptin, 1995). The genetic control of the ventral invagination has been associated with the *snail* and *twist* genes that define the region involved and control the initiation of the biochemical pathway (Leptin, 1995). The kinematics of invagination is characterised by the apical flattening and subsequent apical constriction of the cells in the ventral area (Sweeton et al., 1991; Leptin and Grunewald, 1990; Kam et al., 1991). Eventually, these cells undergo apico-basal elongation, and later shortening, resulting in the invagination sequence shown in Fig. 1. The cell shaping during this process can thus be regarded simplistically as the contribution of two main, localised deformation modes: (i) apical constriction, and (ii) apical-basal elongation (columnari-

---

\* Corresponding Author: Tel. +44 (0) 20 7848 2442, Fax: +44 (0) 20 7848 2932

*Email address:* [mark.miodownik@kcl.ac.uk](mailto:mark.miodownik@kcl.ac.uk) (Mark Miodownik).

*URL:* <http://www.eee.kcl.ac.uk/mecheng/mam> (Mark Miodownik).

sation), resulting in cell wedging and bending of the epithelium (Sweeton et al., 1991; Leptin and Grunewald, 1990; Kam et al., 1991).

Whereas the biochemical characterisation and genetic control of the invagination process have been studied in depth (Leptin, 1995; Barrett et al., 1997; Sweeton et al., 1991; Hacker and Perrimon, 1998; Nikolaidou and Barrett, 2004; Dawes-Hoang et al., 2005), there is a lack of models in the literature that integrate these results into their mechanical environment. However, cell shaping is strongly context dependent (Keller et al., 2003), which motivates us to describe morphogenesis from a mechanical perspective. Moreover, the need for such an approach is not only required for a more complete understanding of morphogenesis, but also because the mechanical information such as strains and stresses, have apparently also an important role in the regulation of certain gene expressions (Gordon, 1999; Farge, 2003; Brouzés et al., 2004; Supatto et al., 2005).

Various models have been devised that address the mechanics of cell movement such as invagination or neurulation (see also the review in Taber (1995)). A common feature in all these models is the presence of trusses as actuators that simulate elements of the cytoskeleton (microtubules and microfilaments). These elements produce the necessary shape changes, mainly apical constriction or axial elongation on certain areas. In the early work of Odell et al. (1981), the trusses of the cells located in the invaginated epithelium have a viscoelastic constitutive law that triggers their apical constriction, and a bistable mechanism that ensures the invagination process. In this way the model generates a wave of constricted cells from the ventral to the dorsal area. Davidson et al. (1995) also tested a global mechanism formed by a continuous microfilament ring around ventral cells that contract the ventral cells. Other mechanical hypothesis include either (i) interactions in the junctions between the cell layer (cell tractoring of plasma membrane (Jacobson et al., 1986)), (ii) interactions cell-extracellular matrix (ECM) such as peripheral intercalation, tangential forces (Clausi and Brodland, 1993; Brodland and Clausi, 1994) or cell crawling

on ECM (Davidson et al., 1995), or (iii) external mechanisms such external forces (Clausi and Brodland, 1993; Brodland and Clausi, 1994) or swelling of apical lamina that forces the ECM to bend, (Davidson et al., 1995).

In contrast, the model proposed here does not use any structural element. We impose in a distributed manner the kinematics of the two main observed modes of *active* deformation observed in *Drosophila* ventral furrow invagination: apical constriction and apico-basal elongation. Superimposed onto this active part, an hyperelastic *passive* deformation takes place, which ensures the continuity and static equilibrium of the material. One advantage of the method is the independence of the final deformed configuration from the material properties, which are in general difficult to measure.

We note that the model does not introduce the causes of the active deformations. These are considered as an internal (chemomechanically transduced) contribution that produce different combinations of the two mentioned components. No interaction forces external to the cell layer are included, other than the presence of the vitelline membrane and the yolk. The former is considered as a rigid surface constraining the deformation, and the latter imposes a constant volume constraint to the volume within the epithelium. As we will show in the results section, the absence of any of these features leads to deformed configurations that do not agree with the observed experimental geometries.

The decomposition of the deformation gradient was originally introduced for elasto-plastic analyses (Lee, 1969). In biomechanics, it has been proposed to distinguish the active and passive contributions by Rodriguez et al. (1993) for the analysis of blood vessels. Analytical results have been included in Rodriguez et al. (1993) and Taber and Humphrey (2001) for simple geometries, and finite element analysis (FEA) of chick embryos and blood vessels are developed in Taber and Perucchio (2000) and Kuhl et al. (2005), respectively. In these applications the term 'active' pertains to cell growth, where as the active stresses

involved in invagination involve cell shape change, so although the method seems very suited for our application, we are modelling a distinctly different type of active mechanism.

## 2 Method

### 2.1 *Deformation gradient decomposition*

We model the permanent (active) deformations and the (passive) hyperelastic deformations as a local quantity applied to the continuum. In other words, no structural elements such as rods are introduced and we treat each point of the epithelial cell layer as being able to produce any of the two main deformation modes involved in invagination: apical constriction and apico-basal cell elongation. In parallel with the division of the epithelial cells in the embryo, the mesoderm (prospective invaginated cells) and the ectoderm, we will divide the epithelium in our model into areas that contribute with different intensity for each active deformation. The geometry and zone division have been measured from experimental cross sections in (Barrett et al., 1997) and are depicted in Fig. 2.

We assume that the initial configuration of the embryo prior to the invagination process is a stress-free configuration. Although some internal stresses may exist at this point, they will be here neglected. As we will show below, the active deformations in our model are independent of the stress level and thus, we would obtain identical results if we considered initial stresses. The initial configuration is a reference state from where the active and elastic deformations will be obtained. Also, although in some situations viscoelastic effects may be relevant, we attempt here to test the main driving forces, and thus, viscous forces are also neglected.

In order to capture the large deformations present in the invagination process, we use finite

strains. By denoting as  $\mathbf{x}$  the current position of a material point, and  $\mathbf{X}$  as its reference (initial) position, the deformation gradient tensor, extensively used in finite elasticity, is given by  $\mathbf{F} = \frac{\partial \mathbf{x}}{\partial \mathbf{X}}$  (Bonet and Wood, 1997; Taber, 2004). We will additionally introduce an intermediate configuration  $\bar{\mathbf{x}}$ , which is the result of applying an active deformation field given by  $\mathbf{F}_p = \frac{\partial \bar{\mathbf{x}}}{\partial \mathbf{X}}$ . The deformation between configurations  $\mathbf{x}$  and  $\bar{\mathbf{x}}$  will be assumed as hyperelastic, with a deformation gradient expressed as  $\mathbf{F}_e = \frac{\partial \mathbf{x}}{\partial \bar{\mathbf{x}}}$ . Hence, the total deformation gradient  $\mathbf{F}$  is split resorting to a multiplicative decomposition with the form  $\mathbf{F} = \mathbf{F}_e \mathbf{F}_p$ . Fig. 3 shows the mentioned relations between the mappings  $\mathbf{F}$ ,  $\mathbf{F}_e$  and  $\mathbf{F}_p$ . The elastic deformation in fact accounts for the compatibility of the deformation, i.e. it precludes material discontinuities in the last deformed configuration represented by  $\mathbf{x}$ .

The stiffness of the epithelium of a sea urchin was measured by a set of experiments by Davidson et al. (1999). From their results we have extrapolated a reference value for the Young modulus of the cell layer in the *Drosophila* as  $E = 1000$  Pa, and we have also assumed a Poisson ratio of  $\nu = 0.3$ . We have adapted these values for our non-linear analysis using the relationships  $\lambda = \frac{\nu E}{(1-2\nu)(1+\nu)} = 576.9 N/m^2$  and  $\mu = \frac{E}{2(1+\nu)} = 384.6 N/m^2$ . Although these formulae are only valid for linear elastic materials, we have used the resulting values of  $\lambda$  and  $\mu$  in the expression of the non-linear strain energy function  $\Psi$  for a Neo-Hookean hyperelastic material, as follows:

$$\Psi = \frac{\mu}{2}(\mathbf{F}_e : \mathbf{F}_e - 3) - \mu \ln J_e + \frac{\lambda}{2}(\ln J_e)^2, \quad (1)$$

where  $J_e = \det(\mathbf{F}_e)$ . The equilibrium of the elastic deformations is obtained by minimising the integral of this energy function in the whole domain of the epithelium. We will show that in our model, when considering a homogeneous constant material, the deformed configurations are very similar regardless of its elastic properties. It has been numerically

tested and shown in the results that for the embryo geometry, the stiffer the material, the larger the values of the stresses, but without any substantial change in the final shape. This is due to the fact that our applied active deformation is independent of the stresses. This avoids having to treat the problem in terms of the active stresses which the cells produce, for which there is no experimental data at the moment, and instead couch the problem in terms of active strains, for which there is data.

The imposed active deformations represent active forces which assume the presence of an energy source in the material. Whether the intensity of this energy source is a function of deformation or stresses is still not clear (Taber and Perucchio, 2000). We circumvent the controversy by applying a linear factor progressively, proportional to a pseudo-time  $\tau$ . The next section explains in detail the form of the applied strains.

In addition, we represent the vitelline membrane as a rigid external ring in 2D, see Fig. 2. This requires a model of the sliding contact conditions of the apical side of the cells onto this membrane. From the numerical standpoint, this contact phenomenon is treated via the use of the master-slave approach (Muñoz and Jelenić, 2004), which avoids Lagrange multipliers or penalty methods, and uses only the minimum set of degrees of freedom.

## *2.2 Active deformations in the finite element context*

In finite element methods, it is a standard practice to use the parametric mapping of the element variables, here denoted by  $\mathbf{J}_\xi$ . In Lagrangian formulations, (Bonet and Wood, 1997), this allows any function of the material coordinates  $\mathbf{X}$  to be expressed as a function of the parametric coordinates  $\boldsymbol{\xi} \in \mathbb{R}^{ndim}$ , where  $ndim$  is the number of dimensions of the problem (2 or 3), and  $\xi_i \in [-1, 1]$ . As it is customary, we will denote the parametric domain as  $\square$ , which is defined by  $\square = \{\boldsymbol{\xi} \in \mathbb{R}^{ndim} | \xi_i \in [-1, 1]\}$ . Fig. 4 illustrates the mapping of  $\mathbf{J}_\xi$ , which in fact will become very useful when applying active deformations.

By resorting to the parametric space, an appropriate deformation field  $\mathbf{J}_p$  can be applied onto the parametric coordinates  $\boldsymbol{\xi}$  which are transformed into  $\bar{\boldsymbol{\xi}}$ . By applying the inverse  $\mathbf{J}_\xi^{-1}$  to the new coordinates  $\bar{\boldsymbol{\xi}}$ , we finally obtain the new material coordinates  $\bar{\mathbf{x}}$ , transformed by the active deformation  $\mathbf{J}_p$ . According to these transformations, depicted in Fig. 5, the active deformation gradient can be expressed as,

$$\mathbf{F}_p = \mathbf{J}_\xi \mathbf{J}_p \mathbf{J}_\xi^{-1}. \quad (2)$$

We can now define a set of suitable applied transformations that represent apical constriction and apico-basal elongation of the parametric domain  $\square$ , denoted by  $\mathbf{J}_{ac}$  and  $\mathbf{J}_{el}$  respectively. Table 1 gives two possible expressions for two-dimensional active deformations, which are used in our numerical expressions. They are written as a function of two parameters  $\tau_1$  and  $\tau_2$  which define the temporal evolution of the active deformation. For  $\tau_i = 0$  no deformation exists in both cases. More explicitly, the deformed parametric domain  $d\bar{\boldsymbol{\xi}}$  is obtained from the undeformed one,  $d\boldsymbol{\xi}$ , as

$$d\bar{\boldsymbol{\xi}} = \mathbf{J}_p d\boldsymbol{\xi}. \quad (3)$$

Depending on whether we are applying apical constriction or apico-basal elongation,  $\mathbf{J}_p = \mathbf{J}_{ac}$  or  $\mathbf{J}_p = \mathbf{J}_{el}$ , respectively. We note that for  $\tau_2 < 0$ , the deformation gradient  $\mathbf{J}_{el}(\tau_2)$  can represent apico-basal shortening. The reader can verify that when using the expressions given in Table 1, the parametric domain is qualitatively deformed according to Fig. 6.

We also note that in the case when a combination of apical-constriction and apico-basal elongation is applied, the resulting deformation gradient may be obtained as  $\mathbf{J}_p = \mathbf{J}_{ac} \mathbf{J}_{el}$ , or  $\mathbf{J}_p = \mathbf{J}_{el} \mathbf{J}_{ac}$ . Although both products lead to different expressions, numerical examples

not shown here demonstrate both choices give very similar results. We have used in our examples the latter expression, i.e.

$$\mathbf{J}_p(\tau_1, \tau_2) = \mathbf{J}_{el}(\tau_2)\mathbf{J}_{ac}(\tau_2) = \begin{bmatrix} (1 + \tau_1\xi_2)(1 + \tau_2) & \tau_1\xi_2(1 + \tau_2) & 0 \\ 0 & \frac{1}{1+\tau_2} & 0 \\ 0 & 0 & 1 \end{bmatrix}. \quad (4)$$

It is worth noting that in all the applied deformations, the volume of the parametric domain is kept constant. This can be shown in 2D using the previous expression  $\mathbf{J}_p(\tau_1, \tau_2)$  as follows:

$$V_{\square} = \int_{\square} d\bar{\xi}_1 d\bar{\xi}_2 = \int_{\square} |\mathbf{J}_p| d\xi_1 d\xi_2 = \int_{\square} (1 + \tau_1\xi_2) d\xi_1 d\xi_2 = \int_{\square} d\xi_1 d\xi_2 + \tau_1 \int_{\square} \xi_2 d\xi_1 d\xi_2 = V_{\square}, \quad (5)$$

where the last identity holds due to the fact that  $\xi_2 \in [-1, 1]$ .

### 3 Numerical Experiments

We performed a systematic series of virtual experiments to investigate the relevance and influence on the global deformation history of (i) the two types of active deformation modes, (apical constriction or apico-basal elongation), (ii) boundary conditions such as the the internal pressure of the yolk and the presence of the rigid vitelline membrane, and (iii) the influence of the material stiffness. The geometry and discretisation used in all the analyses is shown in Fig. 2, which corresponds to the initial undeformed configuration.

Since the displacements are in general smooth, we have taken the size of the element as representative of the global deformation, and small enough to describe accurately the deformed shape of the embryo. We note though that while the apico-basal elongation is independent of the mesh size, apical constriction is dependent on the discretisation. In order to consistently reproduce apico-basal deformations of a cell, no divisions were employed along the radial thickness of the embryo.

### 3.1 Mode contribution

In the first set of experiments the ectoderm and the mesoderm of the embryo were subjected to a monotonically increasing active deformation according to Table 2. To simplify the model, each analysis uses a constant ratio between the parameters  $\tau_1$  and  $\tau_2$ , i.e

$$\alpha = \frac{\tau_1}{\tau_2} = \text{constant}, \quad (6)$$

whenever  $\tau_2 \neq 0$ . A set of numerical tests were performed for different values of  $\alpha$ . The resulting deformed configurations are shown in Fig. 7.

### 3.2 The effect of vitelline membrane and yolk pressure

We also tested the role of the vitelline membrane, assumed as rigid, and the imposed constant volume constraint of the yolk. Three types of analyses were performed with  $\alpha = 4$ . The first with the rigid membrane and the constant volume constraint, a second one where the rigid membrane was absent, and a third with no constant volume constraint. Fig. 8 shows the obtained deformations for the three analyses at  $\tau_1 = 0.6$  and  $\tau_1 = 1.2$ .

### 3.3 Material stiffness

In order to detect any material dependence, material constants  $\lambda$  and  $\mu$  with different orders of magnitude were employed. Fig. 9 shows two of the deformed phenotypes, superimposed with the contour of the circumferential stress component  $\sigma_{\theta\theta}$  of the Cauchy stress tensor. The intermediate values lead to nearly identical deformations and stress values inversely proportional to the material constants  $\lambda$  and  $\mu$ .

## 4 Results and Discussion

Fig. 7 shows the deformed configurations for  $\alpha = 0, 1, 2, 4, 5$  and  $\infty$ . Since  $\alpha = cnst$ , its values and that of  $\tau_1$  or  $\tau_2$  indicated in the figure fully describe the amount of active deformation applied to the embryo. In general, it can be inferred that for  $\alpha < 4$ , the two borders of the ventral furrow remain too open to produce invagination and a large indented area is formed by the mesodermal cells. The same difficulties to close the invaginated cells is encountered for values of  $\alpha > 5$ . In this case, though, a small cavity is created even if the wedge shaped ventral cells are highly constricted. We note that when the analyses were run for larger values of  $\tau_1$  or  $\tau_2$ , no substantial deformed configurations were obtained.

A summary of the influence of the rigid vitelline membrane and the internal pressure of the yolk on invagination geometry is shown in Fig. 8. Although there are no large discrepancies in the level of indentation of the invaginated region, the intermediate (column A1-C1) and final geometries (column A2-C2) are significantly different. The differences in the volume evolution shown in Fig. 10 for the analyses in A1-A2 and C1-C2 confirm this fact. Comparison of the evolution of invagination with the experimental case, Fig. 1, show clearly that effects of rigid vitelline membrane and internal pressure of the yolk should not be ignored. This is supported by the observation that removal of the vitelline

membrane results in the opening of the furrow in a gastrulating embryo *in vivo* (Leptin and Grunewald (1990)).

Thus a set of plausible mechanisms have been identified for the generation of invagination. The combinations tested mostly lead to complete invagination. However we have determined a suitable ratio between apical constriction and apico-basal elongation which causes invagination with a geometry in good qualitative agreement with experiment.

The advantage of the method is that it can parallel the expression of certain genes such as *snail*. The fact that the model without apico-basal elongation ( $\tau_2 = 0$ ) can produce invagination to a certain extent is in agreement with the results in Leptin and Grunewald (1990). Moreover, none of the mechanisms inserted in the model are fully responsible of invagination. Furthermore, the deformed configurations are insensitive to changes in the material parameters, so that the final phenotype remains little changed even when the constants  $\lambda$  and  $\mu$  differ in orders of magnitude. Such behaviour can be interpreted as a mechanism to provide redundancy and robustness to the invagination process.

We have not quantitatively compared our results with those from experiments because the former is fundamentally a 3D phenomenon and so we do not expect a 2D model to capture the exact geometry of a 2D section. The purpose of showing the results from our 2D model is to illustrate the plausibility and rigorousness of our numerical approach. Full quantitative comparisons with experiment will be the subject of our next paper in which we extend the model to 3D.

The aim of our work is to harmonise the hypothesis given at the genetic level with their mechanical counterpart. Both levels form part of the same phenomenon, and their integration may help to elucidate which mechanisms are actually taking part during invagination. Developing such a model is particularly important in light of recent evidence that mechanical regulation can induce the expression of the morphogens during gastrulation (Gordon,

1999; Farge, 2003; Brouzés et al., 2004; Shraiman, 2005). In particular, *twist* expression, necessary to produce apical constriction, is apparently mechanically induced by compression of the epithelium (Farge, 2003; Brouzés et al., 2004). In our model, this would imply that the active deformation is controlled by the state of the stresses associated with the elastic deformation, as the one depicted in Fig. 9. Although it is not difficult to envisage a mechanism that regulates the active deformations according to the level of stresses shown in the Fig. 8, this requires further measurements of the elastic properties of the material which relates the active strains with the stress status. Such measurements have been carried out in Davidson et al. (1999); Wiebe and Brodland (2005).

Work by (Belousov, 1998) shows that active and passive stresses can be experimentally distinguished in some embryos using a number of tissue dissection methods. One method requires conditions in which active stresses can be inhibited (such as the use of moderate cooling, or oxidative inhibitors) so that only the passive stresses remain. A second method involves observing the lag-periods of the post-dissection deformations; the active stresses being assumed to be responsible for the deformations that occur after a finite lag periods, where as the immediate deformations are assumed to be due to passive stresses. Belousov (1998) was able to differentiate between passive and active stresses in a wide number of different species but did not perform experiments on *Drosophila* embryos. However such experiments are clearly possible and we hope that this will provide another method to test our model in the future.

## 5 Conclusions

This paper has described a new numerical model for the analysis of morphogenesis from a mechanical standpoint. The method superimposes onto the elastic deformation the observed phenotypes in the areas where these active modes have been experimentally iden-

tified. The model allows us to test different active deformations imposed in a distributed manner, and apply plausible contributions that lead to the observed final deformations.

We have analysed the invagination process in *Drosophila*, and reproduced the global experimental deformations from local cell activity. We differentiated the necessary permanent deformations, stemming from the active forces of the cytoskeleton, and the passive elastic deformation in a qualitative manner.

We have assumed two observed main modes: apical constriction and apico-basal elongation. After testing different levels of activity for each one of them, we conclude that observed invagination requires a minimum ratio of apical constriction. In addition, the deformation layers of the epithelium are not sufficient to obtain reasonable invaginated shapes; the presence of the vitelline membrane and the constant volume constraint that the yolk imposes must be also taken into account. Three-dimensional versions of the model which can describe better the conservation of volume on the whole embryo are currently under study.

Since other morphogenetic process such as neurulation or optic cup formation are also governed by the presence of an active deformation, the model is extensible to these other processes. Finally, let us note that, having modelled invagination, it would be desirable to model other morphogenetic mechanisms such as intercalation, convergence (Keller et al., 2003) or adhesion phenomena resulting in cell crawling or towing of epithelial cells.

## **6 Acknowledgements**

We would like to thank Buzz Baum for his helpful discussions and suggestions, and Jue Tao for her work in the completion of the results. Jose Muñoz and Kathy Barrett are funded by the Biological and Physical Sciences Research Council (BPRSC) and a Royal Society

University Research Fellowship, respectively. This support is greatly acknowledged.

## Appendix A: Constant Volume Constraint

In order to preserve the the total volume of the yolk  $V_y$  throughout the analysis, a penalty method is used. The total elastic potential of the epithelium  $\Pi_{EL}$  is complemented in the following way:

$$\Pi_{TOT} = \Pi_{EL} + \frac{p}{2}(V_y - V_{y0})^2$$

where  $V_{y0}$  is the initial total volume of the yolk, and  $p$  is a penalty parameter. The volume  $V_y$  can be computed by making use of the divergence theorem as,

$$V_y = \int_V dv = \int_V \frac{1}{3} \text{div}(\mathbf{r}) dv = \frac{1}{3} \int_S \mathbf{r} \cdot \mathbf{n} ds.$$

where  $\mathbf{n}$  is the external normal of the volume boundary, and  $\mathbf{r}$  is the position vector of the boundary. By resorting to the FE spatial discretisation, the last integration can be easily evaluated. We only point out that while computing the Jacobian matrix, all the elements surrounding the internal volume of the yolk become coupled, and thus, the sparseness of the stiffness matrix is reduced.

## References

Barrett, K., Leptin, M., Settleman, J., 1997. The Rho GTPase and a Putative RhoGEF Mediate a Signaling Pathway for the Cell Shape Changes in Drosophila Gastrulation.

Cell 91, 905–915.

Belousov, L. V. 1998. The Dynamic Architecture of a Developing Organism: An Interdisciplinary Approach to the Development of Organisms. Dordrecht, the Netherlands:Kluwer.

Bonet, J., Wood, R., 1997. Non-linear continuum mechanics for finite element analysis. Cambridge University Press.

Brodland, G. W., Clausi, D. A., 1994. Embryonic Tissue Morphogenesis Modeled by FEM. J. Biomech. Engin. 116, 146–155.

Brouzés, E., Supatto, W., Farge, E., 2004. Is mechano-sensitive expression of twist involved in mesoderm formation? Biol. Cell 96, 471–477.

Clausi, D. A., Brodland, G. W., 1993. Mechanical evaluation of theories of neurulation using computer simulations. Development 118, 1013–1023.

Costa, M., Sweeton, D., Wieschaus, E., 1993. The development of *Drosophila melanogaster*. Chapter 8: Gastrulation in *Drosophila*: cellular mechanisms of morphogenetic movements. Cold Spring Laboratory Press.

Costa, M., Wilson, E., Wieschaus, E., 1994. A putative cell signal encoded by the folded gastrulation gene coordinates cell shape changes during *Drosophila* gastrulation. Cell 76 (6), 1075–89.

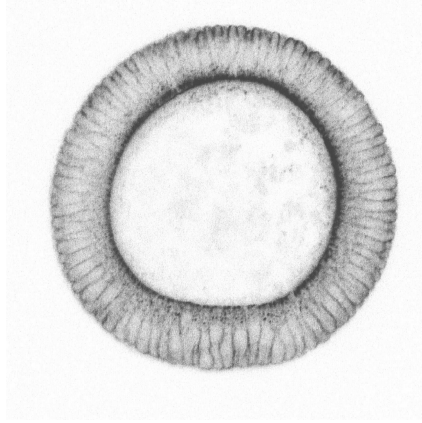
Davidson, L. A., Koehl, M. A. R., Keller, R., Oster, G. F., 1995. How do sea urchins invaginate? Using biomechanics to distinguish between mechanisms of primary invagination. Development 121, 2005–2018.

Davidson, L. A., Oster, G. F., Keller, R., Koehl, M. A. R., 1999. Measurements of Mechanical Properties of the Blastula Wall Reveal Which Hypothesized Mechanisms of Primary Invagination Are Physically Plausible in the Sea Urchin *Strongylocentrotus purpuratus*. Dev. Biology 209, 221–238.

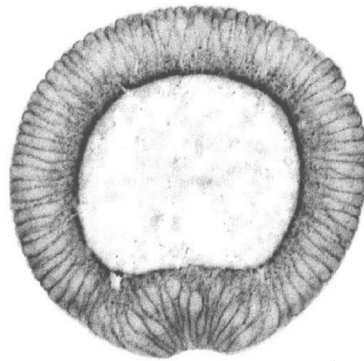
Dawes-Hoang, R., Parmar, K., Christiansen, A., Phelps, C. B., Brand, A. H., Wieschaus, E. F., Sep 2005. *folded gastrulation*, cell shape change and the control of myosin local-

- ization. *Development* 132 (18), 4165–78.
- Farge, E., 2003. Mechanical Induction of Twist in the *Drosophila* Foregut/Stomodaeal Primordium. *Current Biol.* 13, 1365–1377.
- Gordon, R., 1999. The hierarchical genomes and differentiation waves: novel unification of development, genetics and evolution. ”Singapore & London: World Scientific & Imperial College Press”.
- Hacker, U., Perrimon, N., 1998. DRhoGEF2 encodes a member of the Dbl family of oncogenes and controls cell shape changes during gastrulation in *Drosophila*. *Genes Dev.* 12, 274–84.
- Jacobson, A. G., Oster, G., Odell, G. M., Cheng, L. Y., 1986. Neurotation and the cortical tractoring model for epithelial folding. *J. Embryol. Exp. Morph.* 96, 19–49.
- Kam, Z., Minden, J. S., Agard, D. A., Sedat, J. W., Leptin, M., Jun 1991. *Drosophila*, gastrulation: analysis of cell shape changes in living embryos by three-dimensional fluorescence microscopy. *Development* 112 (2), 365–70.
- Keller, R., Davidson, L. A., Shook, D. R., 2003. How we are shaped: The biomechanics of gastrulation. *Development* 71, 171–205.
- Kuhl, E., Himpel, G., Menzel, A., 5-7 September 2005. A kinematic approach towards biological growth within open system thermodynamics. In: *Complas 2005. ECCOMAS Thematic Conference*, Barcelona.
- Lee, E. H., 1969. Elastic-plastic deformation at finite strains. *J. Appl. Mech.* 36, 1–6.
- Leptin, M., 1995. *Drosophila* gastrulation: from pattern formation to morphogenesis. *Annu. Rev. Cell Dev. Biol.* 11, 189–212.
- Leptin, M., Grunewald, B., 1990. Cell shape changes during gastrulation in *Drosophila*. *Development* 110, 72–84.
- Muñoz, J., Jelenić, G., 2004. Sliding contact conditions using the master–slave approach with application on the geometrically non-linear beams. *Int. J. Solids Struct.* 41, 6963–6992.

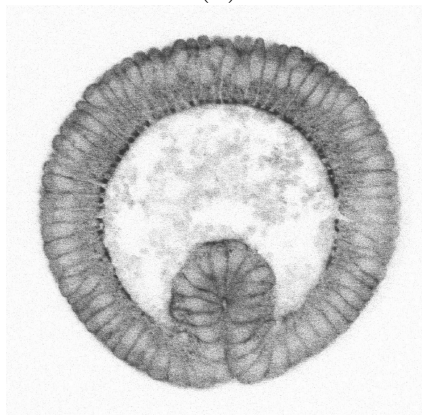
- Nikolaidou, K. K., Barrett, K., Oct 2004. A Rho GTPase signaling pathway is used re-iteratively in epithelial folding and potentially selects the outcome of Rho activation. *Current Biol.* 14 (20), 1822–6.
- Odell, G. M., Oster, G., Alberch, P., Burnside, B., 1981. The mechanical basis of morphogenesis. I. Epithelial folding and invagination. *Dev. Biology* 85, 446–462.
- Parks, S., Wieschaus, E., Jan 1991. The *Drosophila* gastrulation gene *concertina* encodes a G alpha-like protein. *Cell* 64 (2), 447–58.
- Rodriguez, E. K., Hoger, A., McCulloch, A. D., 1993. Stress-dependent finite growth in soft elastic tissues. *J. Biomechanics* 27, 455–467.
- Shraiman, B. I., 2005. Mechanical feedback as a possible regulator of tissue growth. *Proc. Nat. Acad. Sci. USA* 102 (9), 3318–23.
- Supatto, W., Débarre, D., Moulia, B., Brozés, E., Martin, J. L., Farge, E., 2005. In *vivo* modulation of morphogenetic movements in *Drosophila* embryos with femtosecond laser pulses. *Proc. Nat. Acad. Sci. USA* 102 (4), 1047–1052.
- Sweeton, D., Parks, S., Costa, M., Wieschaus, E., 1991. Gastrulation in *Drosophila*: the formation of the ventral furrow and posterior midgut invaginations. *Development* 112, 775–789.
- Taber, L. A., 1995. Biomechanics of growth, remodeling, and morphogenesis. *Appl. Mech. Rev.* 48 (8), 487–545.
- Taber, L. A., 2004. *Nonlinear theory of elasticity: applications in biomechanics*. World Scientific Publ.
- Taber, L. A., Humphrey, L. D., 2001. Stree-modulated growth, residual stresses, and vascular heterogeneity. *J. Biomech. Engin.* 123, 528–535.
- Taber, L. A., Perucchio, R., 2000. Modelling heart development. *J. Elasticity* 61 (8), 165–197.
- Wiebe, C., Brodland, G. W., 2005. Tensile properties of embryonic epithelia measured using a novel instrument. *J. Biomechanics* 38 (10), 2087–2094.



(a)



(b)



(c)

Fig. 1. Successive stages of ventral furrow invagination from experiment. Cells are outlined in a cross-section of the embryo using phalloidin to highlight filamentous actin; (a) cells on the ventral side (bottom) are just beginning to flatten their apical surfaces, (b) ventral cells have constricted their apical surfaces and elongated apico-basally, (c) ventral cells have invaginated.

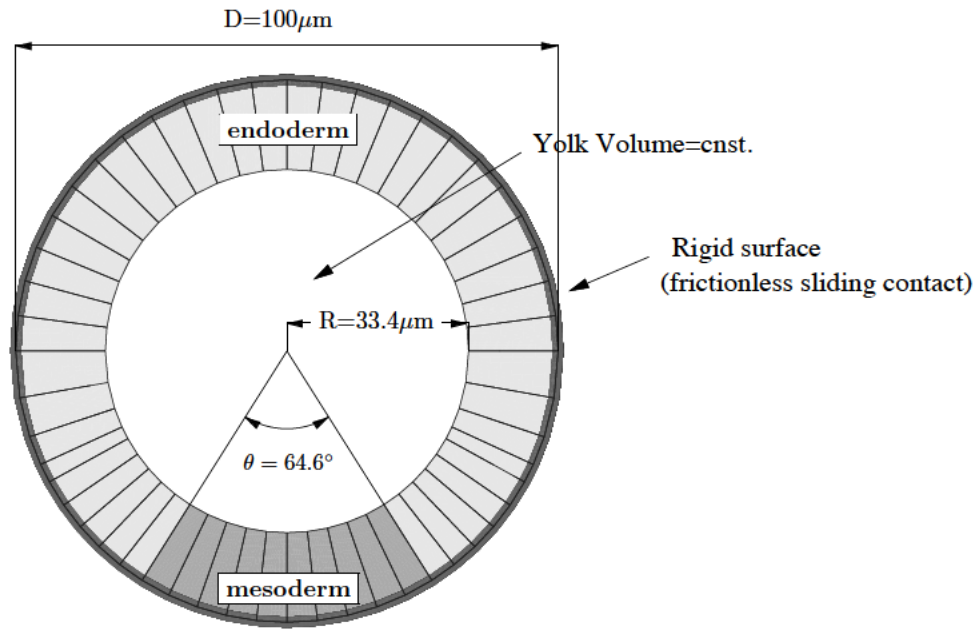


Fig. 2. Geometry of the model and different zones considered.

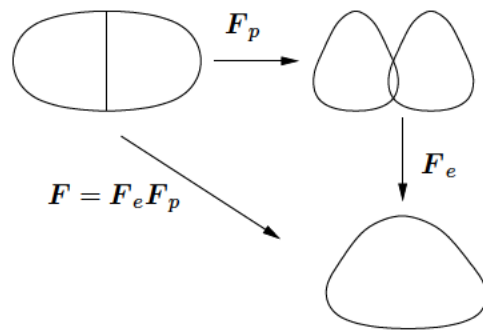


Fig. 3. Scheme of the deformation gradient multiplicative decomposition.

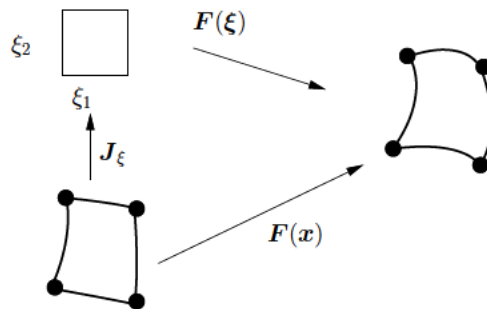


Fig. 4. Scheme of the standard parametric mapping used in finite elements.

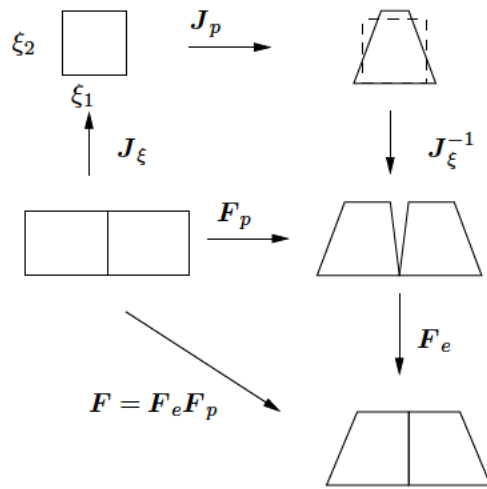


Fig. 5. Scheme of the applied active deformation gradient  $J_p$  within the finite element context.

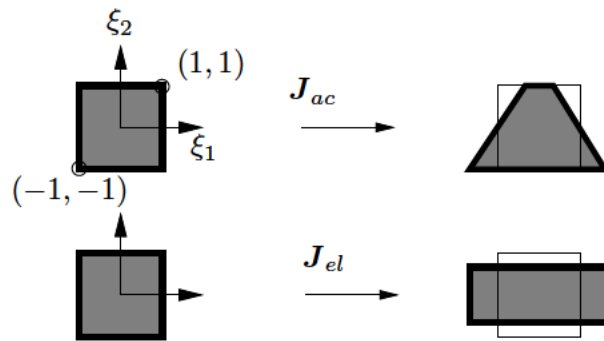


Fig. 6. Apical constriction and apico-basal elongation applied on the parametric domain.

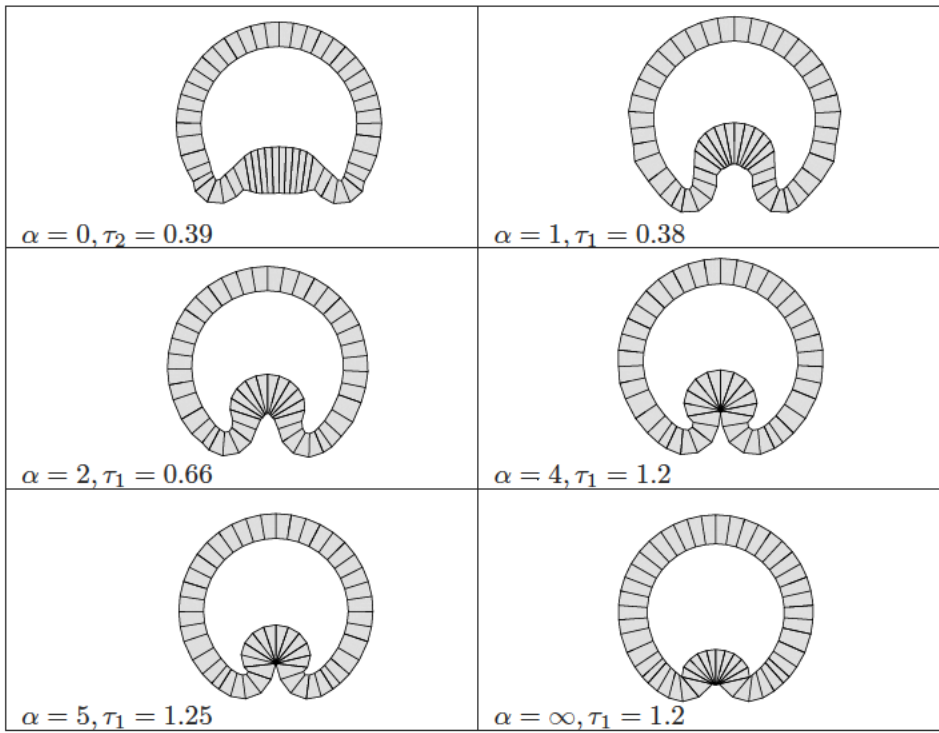


Fig. 7. Deformed configurations using both modes and different values of  $\alpha$ .

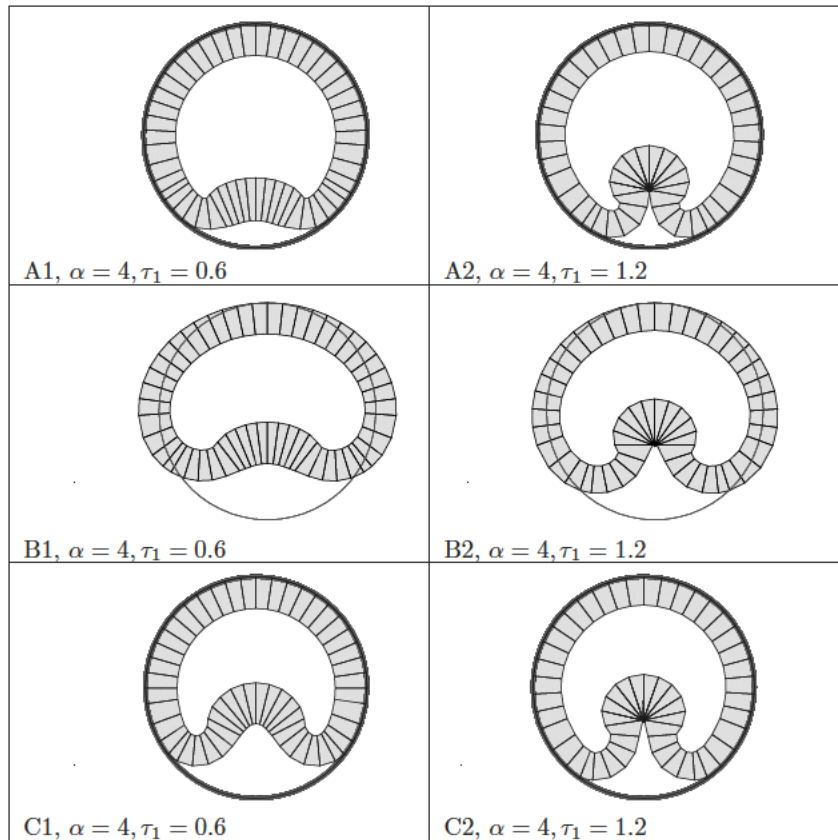


Fig. 8. Deformed configurations for A: vitelline membrane and constant volume constriction, B: no vitelline membrane with constant volume constraint, and C: vitelline membrane with no constant volume constraint.

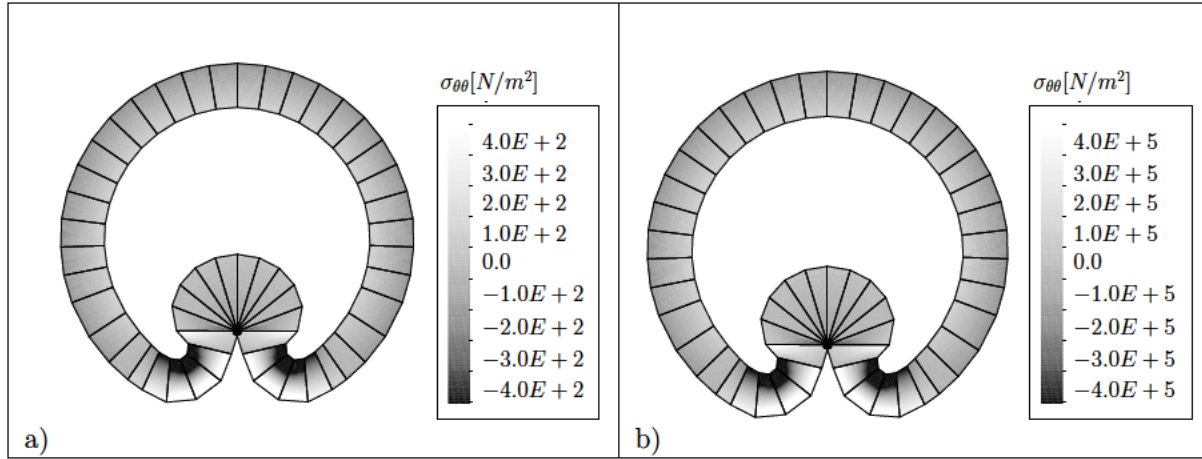


Fig. 9. Different deformed configurations and contours of the circumferential stress component  $\sigma_{\theta\theta}$  of the Cauchy stress tensor for (a)  $\lambda = 576.9 \text{ Pa}$ ,  $\mu = 384.6 \text{ Pa}$  and (b)  $\lambda = 576.9E+03 \text{ Pa}$ ,  $\mu = 384.6E+03 \text{ Pa}$ . Both analyses use  $\alpha = 4$  and are shown for  $\tau_1 = 1.2$ .

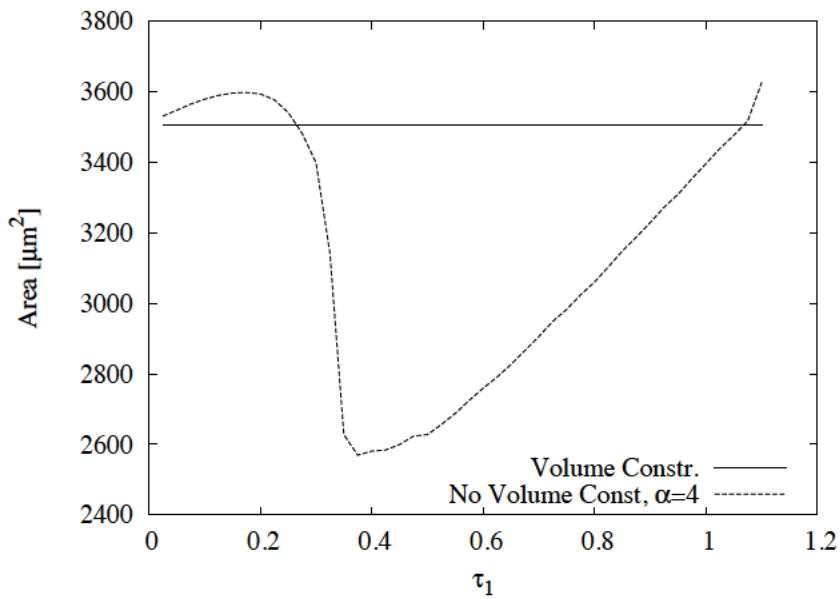


Fig. 10. Evolution of the internal area of the yolk for models with and without the constant volume constraint.

Apical Constr. (AC)	Apico-basal Elong. (AE)
$\mathbf{J}_{ac}(\tau_1) = \begin{bmatrix} 1 + \tau_1 \xi_2 & \tau_1 \xi_1 & 0 \\ 0 & 1 & 0 \\ 0 & 0 & 1 \end{bmatrix}$	$\mathbf{J}_{el}(\tau_2) = \begin{bmatrix} 1 + \tau_2 & 0 & 0 \\ 0 & \frac{1}{1+\tau_2} & 0 \\ 0 & 0 & 1 \end{bmatrix}$

Table 1

Deformation gradients for apical constriction and apico-basal elongation.

Zone	$\mathbf{J}_p(\tau_1, \tau_2)$	Description
Endoderm	$\mathbf{J}_p(0, \tau_2)$	Apico-basal shortening (Radial elongation)
Mesoderm	$\mathbf{J}_p(\tau_1, -\tau_2)$	Apical constr. + Apico-basal elong. (Radial short.)

Table 2

Deformation gradients at each zone of the epithelium.